Journal of Molecular Structure 1016 (2012) 13–21

Contents lists available at SciVerse ScienceDirect

Journal of Molecular Structure

journal homepage: www.elsevier.com/locate/molstruc

Structural characterization of a new dioxamic acid derivative by experimental (FT-IR, NMR, and X-ray) analyses and theoretical (HF and DFT) investigations

G.P. Souza [a,c], C. Konzen [b], T.R.G. Simões [c], B.L. Rodrigues [c], A.F.C. Alcântara [c,*], H.O. Stumpf [c]

[a] Departamento de Química, Universidade Federal de Ouro Preto, Ouro Preto, MG, Brazil
[b] Laboratório de Física Aplicada, Centro de Desenvolvimento da Tecnologia Nuclear, CP 941, 30123-970 Belo Horizonte, MG, Brazil
[c] Departamento de Química, ICEx, Universidade Federal de Minas Gerais, 31270-901 Belo Horizonte, MG, Brazil

ARTICLE INFO

Article history:
Received 27 September 2011
Received in revised form 26 January 2012
Accepted 26 January 2012
Available online 24 February 2012

Keywords:
Molecule-based magnet
Dioxamic acids
Supramolecular chemistry
X-ray crystal structure
NMR analysis
HF and DFT calculations

ABSTRACT

Very few investigations concerning the crystal structure and chemical properties of dioxamic acids have been related in the literature. This work describes the chemical properties of *ortho*-phenylenebis(oxamic acid) (**2**) and its new derivative, hydrogeno *ortho*-phenylenebis(oxamato) benzimidazolium (**3**) using experimental (FT-IR, NMR, and X-ray single crystal diffraction) and theoretical (HF/3-21G* and B3LYP/6-31G* calculations) methodologies. Compound **2** displays intramolecular hydrogen bonding between the hydrogen of an amide group and the oxygen atom of another amide group present in the structure. Compound **3** was prepared by a newly developed synthetic route involving decomposition of the dioxamic acid in solution without the presence of metallic ions. Thermodynamic calculations indicate a process via two successive hydrolyzes of the amide groups of **2**, followed by condensation with formic acid and finally dehydration. The structure of **3** was solved by X-ray single-crystal diffraction and it consists of *meso*-helical chains stabilized by intra and intermolecular hydrogen bonds and π–π stacking interactions.

1. Introduction

Oxamic acids and their ester derivatives are biologically important, showing antiallergic, antirheumatic, and antiinflammatory activities [1,2]. For example, *meta*-phenylenebis(oxamic acid) exhibited significant anti-asthmatic properties, being up to 2500 times more active in rats than disodium cromoglycate, a known agent used in the treatment of bronchial asthma caused by allergy [3]. Bis-oxamato ligands have been used as structural components in molecule-based magnets assemblies, providing efficient coupling among magnetic moments of transition metal ions and lanthanides ions [4,5]. The strategy to prepare such molecule-based magnets with different dimensionalities and physical properties starts with the synthesis of a chelate-effect stabilized monometallic precursor [6–12]. This complex is then used as a building block for magnetic materials since it presents external carbonyl groups capable of bridging metal spin carriers.

Monometallic building blocks have been obtained from the basic hydrolysis of the *ortho*-phenylenebis(oxamic acid ethyl ester) (**1**, Fig. 1), followed by addition of transition metal ions [13,14]. The use of **1** as ligand was not successful in providing new precursors for molecule-based magnets containing Fe^{II}, Fe^{III}, Sn^{II}, or Sn^{IV}. In these cases, the high basicity of the reaction mixture either yields the corresponding metal hydroxide or promotes the formation of the *oxo*-bridged complexes, e.g., $(Et_4N)_4[Fe_2O(opba)_2]\cdot 3H_2O$, with opba standing for *ortho*-phenylenebis(oxamato) [15]. Our research group recently employed an efficient methodology to prepare a molecule-based magnet precursor, $[Fe(H_2opba)(dmso)_2]Cl$, using *ortho*-phenylenebis(oxamic acid) (**2**, Fig. 1) as pro-ligand. This precursor presents the ligand (**2**) in the iminoalcohol tautomeric form, which is not the tautomeric form observed in precursors containing other metallic ions (Cu^{II}, Mn^{II}, Ni^{II}, and Zn^{II}) [16].

The literature has described the synthesis of some dioxamic acids, but very few investigations about their crystal structures, chemical properties, and topological control of their dimensionality have been reported [17]. Recently, a successful example of the topological control of the hydrogen bond-directed self-assembly was reported. The aromatic dioxalamide series of *N*,*N*′-1,*n*-phenylenebis(oxamic acid ethyl ester) molecules with $n = 2$ (H_2Et_2opba), $n = 3$ (H_2Et_2mpba), and $n = 4$ (H_2Et_2ppba) present a supramolecular aggregation of molecules into a duplex (0D), a *meso*-helix (1D) and a brick-wall sheet (2D), respectively. These experimental and theoretical studies show the importance of the two oxalamide moieties as a hydrogen-bonded supramolecular synthons [17].

The application of the oxalamide derivatives as gelling systems has recently attracted considerable attention. The entanglement of

* Corresponding author. Address: Departamento de Química, Universidade Federal de Minas Gerais, Avenida Presidente Antônio Carlos, 6627, Campus Pampulha, Belo Horizonte, Minas Gerais 31270-901, Brazil. Tel.: +55 31 3427 5542 (W), +55 31 3409 5728; fax: +55 31 3409 5700.
E-mail address: aalcantara@zeus.qui.ufmg.br (A.F.C. Alcântara).

0022-2860/$ - see front matter © 2012 Elsevier B.V. All rights reserved.
doi:10.1016/j.molstruc.2012.01.044

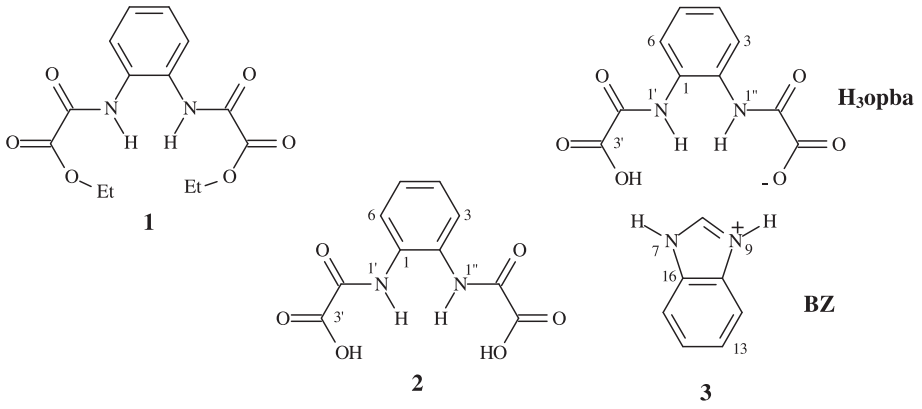

Fig. 1. Chemical structure of the diethyl *ortho*-phenylenebis(oxamato) (**1**), *ortho*-phenylenebis(oxamic) acid (**2**), and hydrogeno *ortho*-phenylene(oxamato) benzimidazolium (**3**; **H_3opba** = hydrogeno *ortho*-phenylenebis(oxamato) and **BZ** = benzimidazolium cation).

the gel fibers, formed by unidirectional self-assembly of these low-molecular organic compounds, can result into three-dimensional networks which traps the solvent. For example, chiral bis(amino acid)oxalamides are able to gel water, as well as a number of low-polarity organic solvents [18,19].

In the present work, the chemical properties of **2** and its new derivative, hydrogeno *ortho*-phenylenebis(oxamato) benzimidazolium (**3**, Fig. 1) were investigated using experimental and theoretical methodologies. Their chemical structures were analyzed from the 1D NMR (^{1}H and ^{13}C) and 2D NMR (^{1}H–^{13}C HMBC and ^{1}H–^{1}H NOESY) at different temperature and in different solvents, including solid-state MAS ^{13}C NMR data. Moreover, a new synthetic method is herein described for the preparation of **3**, whose crystals were suitable for X-ray structure determination. The theoretical studies were based on thermodynamic and carbon chemical shift calculations. Geometry optimizations were carried out using *ab initio* Hartree–Fock (HF) [20] and Density Functional Theory (DFT) [21] methods as recently reported for our studies of other compounds [22,23].

2. Experimental section

2.1. Materials and measurements

Melting points (m.p.) were measured using digital equipment MQAPF-302 Microquimica. Elemental analyses (C, H, N) were performed on a 2400 CHN-Perkin Elmer instrument. Infrared spectra were recorded on a Perkin–Elmer Spectrum GX FTIR spectrophotometer using KBr disks, in the 4000–400 cm^{-1} range. ^{1}H and ^{13}C NMR spectra in solution were recorded on a Bruker AVANCE DRX 400 spectrometer using tetramethylsilane (TMS) as internal standard. The samples (~15 mg) were dissolved in DMSO-d_6 (~0.5 mL). Chemical shifts are given in ppm (δ units). Solid-state NMR spectra were recorded on a Bruker AMX 400 wide-bore NMR spectrometer using a commercial triple resonance MAS 4 mm probe. Proton-decoupled ^{13}C MAS NMR spectra were acquired using cross polarization [24]. Typical acquisition parameters were the following: spin lock time 2.0 ms, recycle delay 3 s, ^{1}H B1 field 91 kHz, 3072 data points, 25,000 acquisitions, and spectral width of 50 kHz. The spectra were acquired at 298 K with a spinning speed of 10 kHz. Adamantane was used as reference (high field signal at 29.5 ppm).

One single crystal of **3** was chosen and mounted on an Enraf–Nonius Kappa-CCD diffractometer equipped with graphite monochromator. Mo Kα (λ = 0.71073 Å) radiation was used in the experiment. The final unit cell parameters were based on all reflections. Data collection used the COLLECT program [25]. Integration and scaling of the reflections were performed with the HKL Denzo–Scalepack system of programs [26]. 3424 Independent reflections resulted from this integration. The absorption correction was tried, but did not improve the model: the crystal is small, as well as its absorption coefficient. 2911 Reflections with positive intensities were merged and used in the structure resolution and refinements. The structure was solved by direct methods with SHELXS-97 [27]. The model was refined by full-matrix least squares based on F^2, through SHELXL-97. All atoms were anisotropically refined. Hydrogen atoms bonded to carbon were stereochemically positioned and refined using the ridging model. Hydrogen atoms of the aromatic rings were set isotropic with a thermal parameter 20% greater than the equivalent isotropic displacement parameter of the atom in which each one is bonded. Hydrogen atoms H711 and H712, which are respectively bonded to N11 and N12, were found on the Fourier difference maps and fixed. Hydrogen atoms bonded to oxygen were also found in the Fourier difference synthesis. The hydrogen atoms HO1 and HO5 were located in special position (inversion center and two-fold axis, respectively), with occupancy factor fixed in 0.5. Their positions and isotropic displacement parameters were fixed. Experimental features are summarized in Table 1.

Table 1
Crystal data and refinement results for **3**.

$C_{11.33}H_{9.33}N_{2.67}O_4$	F_{000} = 1536
M_r = 246.88	D_x = 1.542 Mg m^{-3}
Hall symbol: -C 2yc	Mo Kα radiation, λ = 0.71073 Å
a = 31.299 (4) Å	α = 90°
b = 5.5320 (6) Å	β = 125.454 (6)°
c = 22.623 (4) Å	γ = 90°
V = 3190.8 (7) Å^3	0.068 × 0.213 × 0.048 mm
Z = 8	μ = 0.12 mm^{-1}
Kappa CCD diffractometer	R_{int} = 0.096
Radiation source: fine-focus sealed tube	θ_{max} = 24.7°
Monochromator: graphite	θ_{min} = 2.2°
T = 150 (2) K	h = −35 → 36
3624 Measured reflections	k = −5 → 6
2403 Independent reflections	l = −26 → 26
1056 Observed reflections ($I > 2\sigma(I)$)	
Refinement on F^2	Least-squares matrix: full
$R[F^2 > 2\sigma(F^2)]$ = 0.061	$w = 1/[\sigma^2(F_o^2) + (0.0243P)^2]$ where $P = (F_o^2 + 2F_c^2)/3$
$wR(F^2)$ = 0.127	$(\Delta/\sigma)_{max} < 0.001$
S = 0.89	$\Delta\rho_{max}$ = 0.28 and Å^{-3}
2403 Reflections	$\Delta\rho_{min}$ = −0.30 and Å^{-3}
245 Parameters	Extinction correction: none

All chemicals were of reagent grade quality, purchased from commercial sources, and used as received. The compound *ortho*-phenylenebis(oxamic acid ethyl ester) (**1**) was prepared as reported in the literature [13,14].

2.2. Synthesis of the compounds

Synthesis of *ortho*-phenylenebis(oxamic acid) (**2**) (adaptation of a method described elsewhere) [14]. An aqueous solution of NaOH 0.1 mol/L (14.3 mL; 1.43 mmol) was added dropwise to a suspension of **1** (200.5 mg; 0.65 mmol). After vigorous stirring for 30 min at 60 °C, the reaction mixture was cooled to room temperature and then distilled water (25 mL) and a solution of HCl 1.2 mol/L (about 1.8 mL; 2.16 mmol) were added until pH ~ 1 was achieved. The white solid obtained was filtered, washed with cold water, and finally dried under reduced pressure to give 127.0 mg (yield 72%) of **2** as a white crystalline solid. M.p. 250 °C (decomp.); IR (KBr, ν_{max} in cm^{-1}) ν 3451 (ν_{O-H}), 3299 (ν_{N-H} asym.), 3246 (ν_{N-H} sym.), 3050–3000 (ν_{CH}), 1775 ($\nu_{C=O}$), 1672 (amide I), 1557 (amide II), 1380 (δ_{O-H}), 1295 (δ_{C-O-H} in plane), 1188 (ν_{C-O}), and 748 (δ_{C-H} out-of-plane); ^{1}H NMR (400 MHz, DMSO-d_6) δ_H 10.35 (ls; 2H; NH), 7.60 (dd, J = 3.6 and 5.6 Hz; 2H; H-3/6), and 7.29 (dd, J = 3.6 and 5.6 Hz; 2H; H-4/5); ^{13}C NMR (100 MHz, DMSO-d_6) δ_C 161.6 (C-3′/3″), 156.8 (C-2′/2″), 129.6 (C-1/2), 126.1 (C-4/5), and 125.4 (C-3/6). Anal. Calcd. for $C_{10}H_8N_2O_6$ (MM = 252.18 g/mol): C, 47.6%; H, 3.2%; N, 11.1%. Found: C, 46.1%; H, 3.2%; N, 10.9%.

Synthesis of hydrogeno *ortho*-phenylenebis(oxamato) benzylmidazolium (**3**). Compound **2** (10.0 mg; 0.04 mmol) was dissolved in 2 mL of DMSO. Colorless single crystals of **3** were obtained after 2 months of standing at room temperature and in complete absence of light. The product was collected by filtration, washed with ethanol, and dried under vacuum to give 2.3 mg (yield 32%). M.p. 270 °C (decomp.); IV (KBr, ν_{max} in cm^{-1}) ν 3467 (ν_{O-H}), 3162 (ν_{NH} asym.), 3105 (ν_{N-H} sym.), 3046 (ν_{C-H} arom.), 2967, 2881, 2776 (ν_{N+-H}), 1711 ($\nu_{C=O}$), 1682 (band I of amide), 1616 (band II of amide), 1474 ($\nu_{carboxyl}$ asym.), 1419 ($\nu_{carboxyl}$ sym.), 1393 (δ_{O-H}), 1250 (ν_{C-O}), 855 (δ_{N-H}, out-of-plane), 753, and 703 (δ_{C-H} out-of-plane). The crystal data and refinement for **3** are shown in Tables 1–4.

Table 2
Fractional atomic coordinates and equivalent isotropic displacement parameters of non-hydrogen atoms (Å^2).

	x	y	z	U^*_{iso}/U_{eq}
O1	0.03435 (12)	0.8685 (6)	0.04798 (18)	0.0313 (10)
O2	0.02584 (13)	0.6611 (6)	−0.0442 (2)	0.0372 (10)
O3	0.11147 (12)	0.5627 (6)	0.14348 (19)	0.0321 (10)
O5	0.03343 (12)	−0.0180 (6)	−0.18399 (18)	0.0306 (9)
O4	0.06108 (13)	0.3193 (6)	−0.20844 (19)	0.0360 (10)
O6	0.13121 (14)	0.3839 (7)	−0.05900 (19)	0.0407 (11)
N1	0.10005 (14)	0.3557 (7)	0.0471 (2)	0.0266 (11)
N2	0.10300 (15)	0.0265 (8)	−0.0440 (2)	0.0274 (11)
N11	0.09554 (16)	0.7218 (8)	−0.2353 (3)	0.0353 (12)
N12	0.09981 (16)	1.0215 (7)	−0.2942 (2)	0.0318 (12)
C1	0.04529 (19)	0.6980 (10)	0.0206 (3)	0.0312 (14)
C2	0.08952 (19)	0.5329 (10)	0.0781 (3)	0.0286 (14)
C3	0.13905 (17)	0.1754 (9)	0.0796 (3)	0.0199 (12)
C4	0.17494 (17)	0.1535 (9)	0.1537 (3)	0.0235 (13)
C5	0.21179 (17)	−0.0303 (9)	0.1817 (3)	0.0259 (13)
C6	0.21238 (18)	−0.1960 (9)	0.1367 (3)	0.0274 (13)
C7	0.17645 (18)	−0.1739 (9)	0.0626 (3)	0.0254 (13)
C8	0.14053 (19)	0.0119 (9)	0.0340 (3)	0.0245 (13)
C9	0.10258 (18)	0.2067 (10)	−0.0842 (3)	0.0258 (13)
C10	0.06200 (19)	0.1735 (10)	−0.1672 (3)	0.0289 (13)
C11	0.0725 (2)	0.8295 (11)	−0.3000 (3)	0.0373 (15)
C12	0.1404 (2)	0.8539 (10)	−0.1851 (3)	0.0282 (14)
C13	0.17660 (19)	0.8269 (9)	−0.1119 (3)	0.0290 (13)
C14	0.21645 (19)	0.9960 (10)	−0.0768 (3)	0.0356 (15)
C15	0.2187 (2)	1.1834 (10)	−0.1152 (3)	0.0328 (14)
C16	0.18213 (19)	1.2184 (9)	−0.1891 (3)	0.0315 (14)
C17	0.14303 (19)	1.0439 (9)	−0.2227 (3)	0.0236 (13)

Table 3
Selected geometric parameters for H_4opba (Å, °).

O1—C1	1.280 (6)	C4—C3	1.379 (6)
O1—HO1	0.8400	C17—C12	1.384 (7)
O3—C2	1.227 (6)	C17—N12	1.387 (6)
O5—C10	1.293 (6)	C17—C16	1.389 (6)
O5—HO5	1.230 (4)	C1—C2	1.535 (7)
O4—C10	1.221 (6)	C4—C5	1.385 (6)
O6—C9	1.223 (5)	C7—C8	1.376 (6)
N1—C2	1.354 (6)	C7—C6	1.379 (6)
N1—C3	1.409 (5)	N12—C11	1.320 (6)
N1—H71	0.8800	N12—H712	0.880 (4)
N2—C9	1.344 (6)	C5—C6	1.378 (6)
N2—C8	1.447 (6)	C9—C10	1.551 (7)
N2—H72	0.8800	C15—C14	1.381 (7)
O2—C1	1.234 (6)	C15—C16	1.385 (7)
N11—C11	1.340 (6)	C3—C8	1.394 (6)
N11—C12	1.394 (6)	C12—C13	1.368 (7)
N11—H711	0.915 (4)	C13—C14	1.383 (6)
C1—O1—HO1	109.5	O4—C10—O5	127.7 (5)
C10—O5—HO5	107 (3)	O4—C10—C9	119.1 (5)
C2—N1—C3	129.7 (4)	O5—C10—C9	113.2 (5)
C9—N2—C8	123.3 (4)	C14—C15—C16	123.7 (5)
C9—N2—H72	118.4	C4—C3—C8	119.3 (5)
C8—N2—H72	118.4	C4—C3—N1	123.1 (5)
C11—N11—C12	107.8 (4)	C8—C3—N1	117.6 (4)
C11—N11—H711	135.9 (5)	C13—C12—C17	121.5 (5)
C12—N11—H711	115.9 (5)	C13—C12—N11	131.7 (5)
C12—C17—N12	106.4 (4)	C17—C12—N11	106.8 (4)
C12—C17—C16	122.7 (5)	C7—C8—C3	120.3 (5)
N12—C17—C16	130.9 (5)	C7—C8—N2	118.7 (5)
O2—C1—O1	127.6 (5)	C3—C8—N2	121.0 (5)
O2—C1—C2	119.3 (5)	O3—C2—N1	126.0 (5)
O1—C1—C2	113.0 (5)	O3—C2—C1	122.8 (5)
C3—C4—C5	119.7 (5)	N1—C2—C1	111.2 (5)
C8—C7—C6	120.4 (5)	C5—C6—C7	119.2 (5)
C11—N12—C17	109.0 (5)	N12—C11—N11	110.0 (5)
C11—N12—H712	129.5 (5)	N12—C11—H11	125.0
C17—N12—H712	121.5 (5)	N11—C11—H11	125.0
C6—C5—C4	121.0 (5)	C12—C13—C14	117.4 (5)
O6—C9—N2	124.2 (5)	C15—C14—C13	120.3 (5)
O6—C9—C10	121.5 (5)	C15—C16—C17	114.4 (5)
N2—C9—C10	114.3 (5)		

Table 4
Hydrogen bond parameters (Å, °).

D—H—A	d(D—H)	d(H···A)	d(D···A)	<DHA
O1—HO1—O1^1	0.84	1.618	2.457 (7)	176.6
O1—HO1—O2^1	0.84	2.670	3.184 (5)	120.9
N1—H7—O2	0.88	2.186	2.636 (5)	111.3
N1—H71—O6	0.88	2.623	3.074 (5)	112.9
N2—H72—O2^2	0.88	2.436	3.148 (5)	138.3
O5—HO5—O5^3	1.230 (4)	1.230 (4)	2.459 (6)	176 (6)
O5—HO5—O4^3	1.230 (4)	2.410 (5)	3.131 (5)	115 (3)
N11—H711—O4	0.915 (4)	1.805 (3)	2.693 (5)	162.7(3)
N12—H712—O3^4	0.880 (4)	2.033 (3)	2.830 (5)	150.1(3)
N12—H712—O1^4	0.880 (4)	2.301 (3)	2.972 (5)	133.0(3)

Symmetry codes: (1) −x, −y + 2, −z; (2) x, y − 1, z; (3) −x, y, −z − 1/2; (4) x, −y + 2, z − 1/2.

3. Computational details

Theoretical studies were carried out using the Gaussian03W software package [28]. HF and DFT geometry optimizations were performed using the geometries previously obtained by the PM3 semi-empirical method [29]. BLYP and B3LYP functionals with the standard Pople's split valence 6-31G* basis set were used in

the DFT calculations [30–34]. The optimized geometries were characterized as true minima on the potential energy surface (PES) with all harmonic frequencies being real. The electronic-nuclear energies (E) were calculated by means of the HF and DFT methods. Solvent effect (DMSO, $\varepsilon = 46.7$) in the geometry optimizations were taken into consideration using the Polarizable Continuum Model (PCM) [35,36] as implemented in the HF/6-31G* and DFT/B3LYP/6-31G* Gaussian03 software package.

DFT/BLYP/6-31G* optimized geometries of **2** were used for the carbon chemical shift calculations. Values of calculated carbon chemical shifts (σ_C) of **2** were obtained in relation to the corresponding DFT/BLYP/6-31G* calculated values for tetramethylsilane (σ_C 190.90). For structure **3**, the HF/6-31G* method was used. In this case, the σ_C value for tetramethylsilane was σ_C 201.19. Correlations between σ_C values and experimental carbon chemical shifts (δ_C) were obtained using software package Origin™ Standard 7.5. The σ_C and δ_C values were plotted on x and y axes, respectively. Correlation curves were given as linear fits with correlation coefficients (R^2) and standard deviations (SDs) furnished by the program itself.

The formation of **3** from **2** was investigated through thermodynamic calculations according to Eq. (1). It is worth considering the whole amount of reaction energy (ΔG^{total}) as the sum of three parts: electronic plus nuclear repulsion energy (ΔE^{ele}), DMSO solvation energy (ΔE^{solv}), and thermal correction to the Gibbs free energy (ΔG^{therm}). The thermal contribution was estimated using the ideal gas model and calculated harmonic vibrational frequencies to estimate the zero-point energy correction (ZPE) and the correction due to the thermal population of the vibrational levels.

$$\Delta G^{total} = \Delta E^{ele} + \Delta E^{solv} + \Delta G^{therm} \quad (1)$$

4. Results and discussion

The IR spectrum of **2** shows absorptions at 3299 (ν_{N-H} asym.), 3246 (ν_{N-H} sym.), 1672 (amide I band), and 1557 cm^{-1} (amide II band) which are characteristic of secondary amides. The absorptions at 3451 (ν_{O-H}), 1775 ($\nu_{C=O}$), 1380 (δ_{O-H}), 1295 (δ_{C-O-H} in plane), and 1188 cm^{-1} (ν_{C-O}) are characteristic of carboxylic acid groups. Absorptions at 3050–3000 (ν_{C-H}) and 748 cm^{-1} (δ_{C-H} out-of-plane) are indicative of the presence of aromatic rings.

The ^{1}H NMR spectrum of **2** in DMSO-d_6 at 300 K shows multiplicity of signals at the aromatic hydrogen region which is characteristic of AA′–BB′ spin systems. The singlet signal of hydrogen at δ_H 10.35 (N—H) shows HMBC correlations with the carbon signals at δ_C 156.8 (C-2′/2″, via ^2J), 129.6 (C-1/2, via ^2J), and 125.4 (C-3/6, via ^3J) and also shows NOESY correlations with the multiple signals of hydrogen at δ_H 7.60 (H-3/6). These multiple signals of hydrogen, in its turn, show HMBC correlations with the carbon signals at δ_C 129.6 (C-1/2, via ^2J) and 126.1 (C-4/5, via ^2J). Finally, the hydrogen signal at δ_H 7.29 (H-4/5) shows HMBC correlations with the carbon signals at δ_C 129.6 (C-1/2, via ^3J) and 126.1 (C-4/5, via ^2J). These 1D and 2D NMR data are consistent to the chemical structure of **2**.

^{1}H NMR spectrum of **2** in solution of DMSO-d_6:MeOD (4:1) at 300 K shows a low field signal at δ_H 10.37 ppm and a weak hydrogen resonance appears at δ_H 10.32 ppm, both these signals may be attributed to hydrogen in carboxylic acid groups of two distinct conformations. Moreover, the ^{13}C NMR spectrum of **2** also shows lower signals at δ_C 156.6, 129.5, and 125.3 which are respectively attributed to the carbon atoms C-2′/2″, C-1/2, and C-3/6 of other conformation of **2**. The solid-state MAS ^{13}C NMR spectrum of **2** (Fig. 2) shows weak signals near δ_C 162.0 and 156.0 which may be respectively attributed to C-3′/3″ and C-2′/2″ of the secondary conformer. However, these low-intensity signals are not observed in the ^{13}C NMR spectrum of **2** in DMSO-d_6 at 343 K. As a result, the conformations interconvert too quickly to be resolved on the NMR time scale when the temperature is near 40 °C higher than the room temperature.

B3LYP/6-31G* geometry optimizations were employed to a conformational search of **2**. Two optimized geometries were obtained (**2a** and **2b**, Fig. 3). Geometry **2a** ($E = -946.55156779$ a.u.) shows intramolecular hydrogen bond between the hydrogen of the amide group of a substituent and the oxygen of the amide group of the other one. Geometry **2b** ($E = -946.54910890$ a.u.) shows a C_2 symmetry axis collinear with the aromatic ring plane and the hydrogen atoms of both the amide groups spatially close to each other.

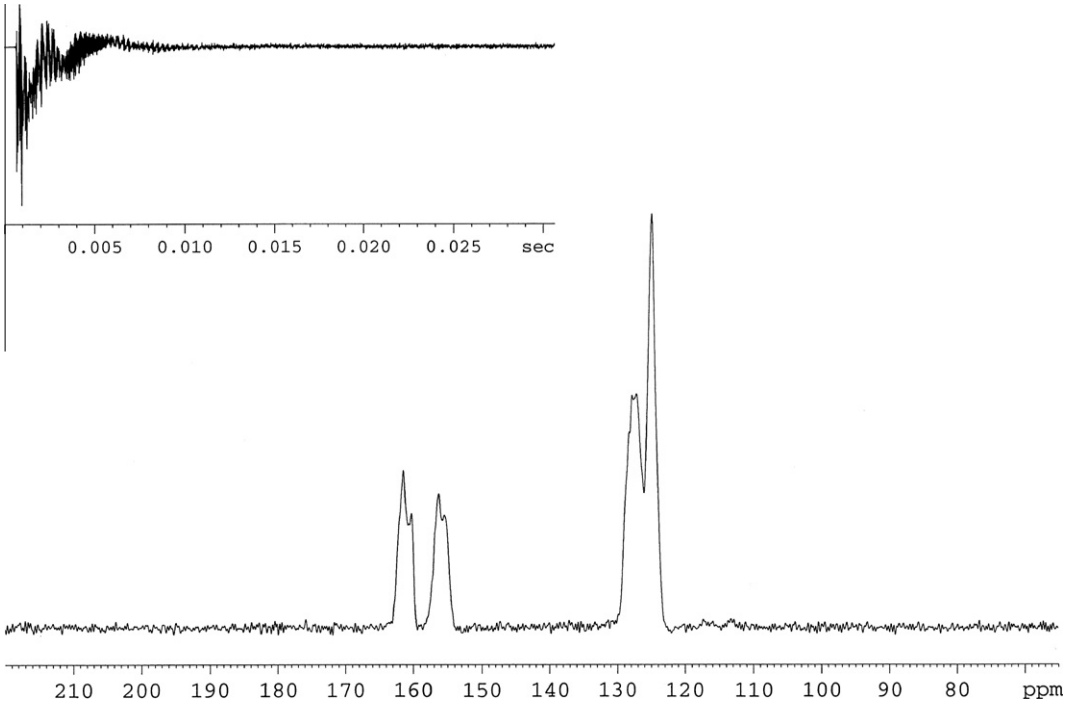

Fig. 2. Solid-state MAS ^{13}C NMR of **2** (100 MHz; adamantane).

B3LYP/6-31G* carbon chemical shift calculations were performed to **2a** and **2b**. The calculated σ_C values of both the geometries were correlated with the experimental chemical shift values obtained from the high-intensity signals in the ^{13}C NMR spectrum of **2**. The geometry **2b** (R^2 = 0.9963 and SD = 1.443) shows higher correlations than the geometry **2a** (R^2 = 0.9943 and SD = 1.695). The thermodynamic calculations indicate **2a** as the predominant conformer while the chemical shift calculations indicate the contrary, i.e., **2b** as the predominant conformer. In previous work, results obtained from carbon chemical shift calculations were verified by their accordance to experimental data [23]. Thus, based on the results from the carbon chemical shift calculations, geometry **2b** may be considered to be the predominant conformer.

The IR spectrum of **3** shows absorptions at 3162 (ν_{N-H} asym.) and 3105 cm^{-1} (ν_{N-H} sym.) characteristic of N—H in hydrogen bonding and absorptions at 2967, 2881, and 2776 cm^{-1} characteristic of N^+—H stretch. The absorption at 1682 cm^{-1} may be attributed to R_2C=NR stretch of imine groups. These IR absorptions are

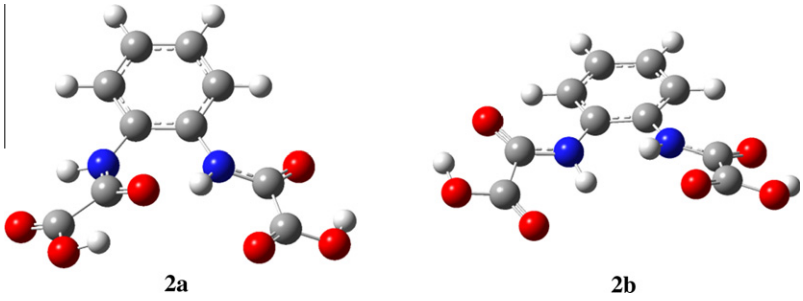

Fig. 3. Optimized geometries of **2**, using BLYP/6-31G* calculations for structures in the gaseous phase.

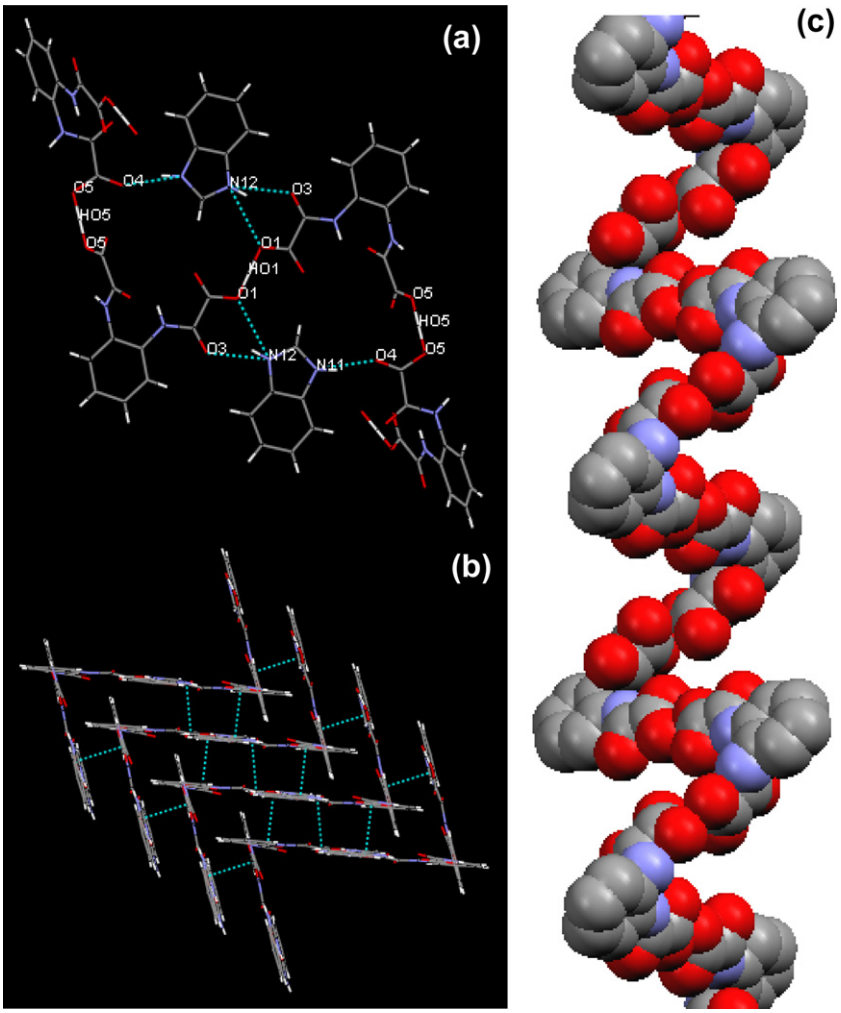

Fig. 4. Representations: (a) plane formed by hydrogen bonding, showing the involved atoms in these interactions, (b) π–π interactions among adjacent chains – benzene–benzene ring distance of 3.874 Å, and (c) crystal packing with chain along the axis *c*, showing hydrogen bond (N—H···O and O—H—O). In the left representation the BZ molecules were omitted.

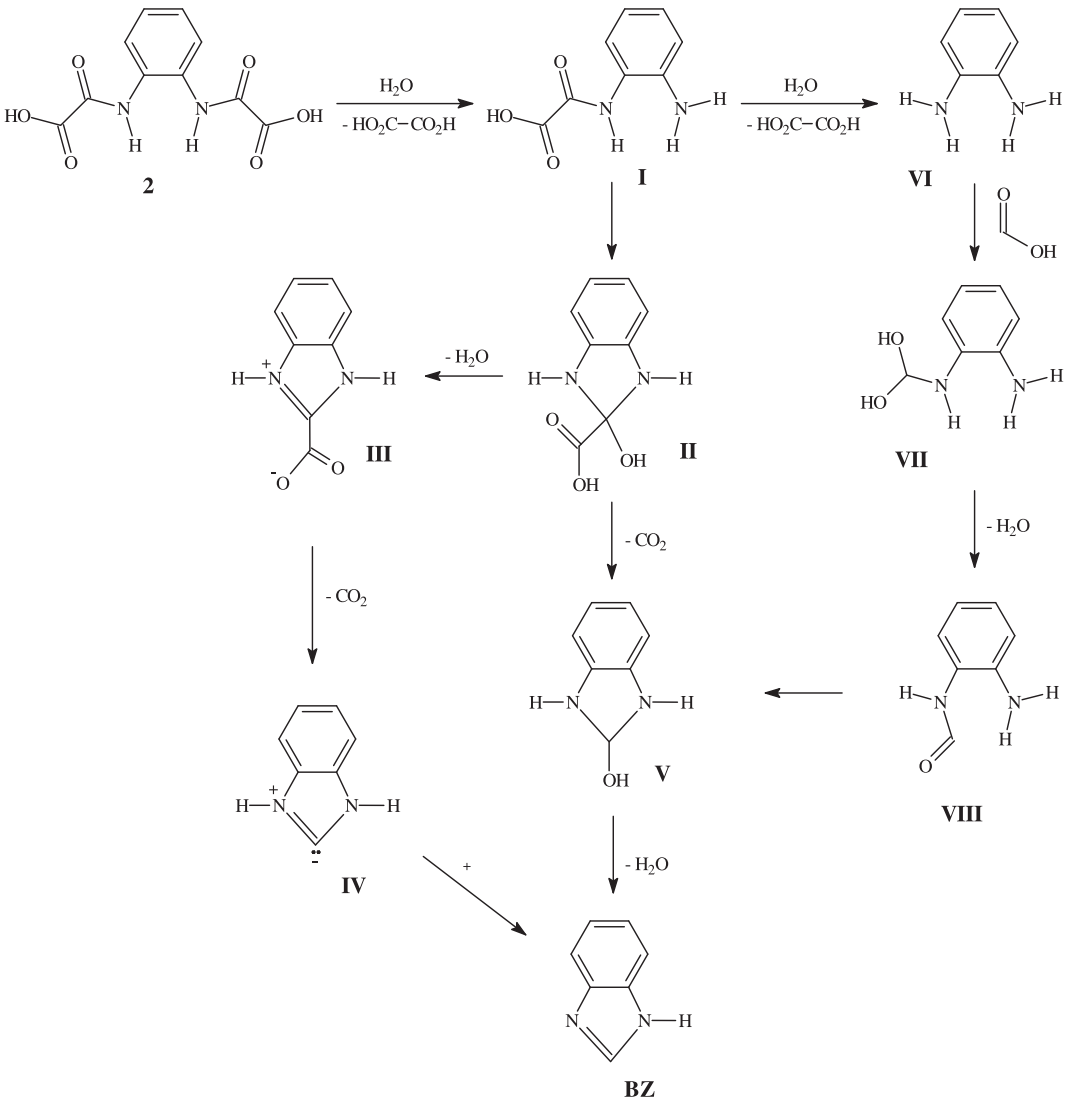

Fig. 5. Sequences of reaction steps proposed to formation of **BZ** from **2**: sequence A (**2** → **I** → **II** → **III** → **IV** → **BZ**), sequence B (**2** → **I** → **II** → **V** → **BZ**), and sequence C (**2** → **I** → **VI** → **VII** → **VIII** → **V** → **BZ**).

in agreement with the chemical structure of an imidazoline cation. Absorptions at 1474 and 1419 cm^{-1} may be attributed to stretching frequencies of the carboxylate group.

The absorptions attributed to C=O stretch in the IR spectrum of **3** ($\nu_{C=O}$ = 1711 cm^{-1}) display lower frequency in relation to the corresponding absorption for **2** ($\nu_{C=O}$ = 1775 cm^{-1}). On the other hand, the absorption attributed to C—O stretch in the IR spectrum of **3** (ν_{C-O} = 1250 cm^{-1}) displays higher frequency as compared with the corresponding absorption in the IR spectrum of **2** (ν_{C-O} = 1188 cm^{-1}). Both the absorption frequency variations provide evidence for the presence of carboxylate groups in the structure of **3**, produced by the proton-transfer reaction from the oxamic acid to the benzylimidazole nitrogen. In fact, some imidazole-type rings show proton conductivity and the structural reorganization occurs by hydrogen bonds-breaking and -making processes [37,38]. These properties are important for preparing proton-conducting membranes which may be usually used as fuel cell [39].

The asymmetric unit of **3** shows the ions benzimidazolium (**BZ**) and hydrogeno *ortho*-phenylenebis(oxamato) (**H_3opba**), as shown in Fig. 1. The hydrogen atoms HO1 and HO5 are located in special positions: HO1 in the inversion center and HO5 on a two-fold axis. Crystal data and refinement results are shown in Tables 1 and 2. Geometric parameters and hydrogen bonding parameters are shown in Tables 3 and 4, respectively. The **H_3opba** anionic unities are connected through strong hydrogen bonds O1—HO1—O1 and O5—HO5—O5 (Table 4), forming an infinite chain parallel to the *c*-direction (Fig. 4a). The alternance between the two-fold axis through HO5 and the inversion center through HO1 of this infinite chain results in a *meso*-helical structure. The interactions involving the **BZ** cations are also important for the crystal packing: this cation is involved in one normal (N11—H711—O4) and two bifurcated (N12—H712—O3 and N12—H712—O1) hydrogen bonds. An weak intramolecular interaction N7—H71—O2 is also observed, The π–π stacking interactions between adjacent chains are also important for the crystal packing (Fig. 4b). The hydrogen bonds among asymmetric units of **3** lead to formation of its crystal structure having an infinity helical chain along the axis *c* (Fig. 4c), in which the *meso*-helical form occurs by supramolecular packaging process. The double helices of the DNA and the α-helices of protein and biopolymers, as α-amilose and cicloamilose, furnish interesting biological examples of helical systems [40,41]. HF/3-21G* geometry optimizations were performed to a *meso*-helical polymeric chain containing 20 units of **3**, with starting geometry generated

from the X-ray single crystal data. The optimized geometry shows destructuration of the *meso*-helical form of the starting geometry. These results indicate that van der Waals, electrostatic interactions, hydrogen bonding, and π–π inter-chain interactions almost certainly play a key role in the aggregation of the polymeric units that provides the *meso*-helical crystal structure of **3**.

The crystal structure of the *N*,*N*′-1,3-phenylenebis(oxamic acid ethyl ester), H_2Et_2mpba, shows a *meso*-helical chain formed by hydrogen bond among the hydrogen of the amide groups and the oxygen of the carboxylic groups [42]. The single crystal X-ray diffraction analysis and theoretical calculations indicated that the helical nature and hydrogen bonding interactions are important for aggregation during the crystal growth of H_2Et_2mpba. In the case of **3**, hydrogen bonds between **BZ** and **H3opba** units lead to formation of rings which give additional stability to its crystal structure. The significant π–π stacking interactions between the neighbor chains are suggested by the benzene–benzene ring distance of 3.874 Å [43]. This information is important to crystal engineering science since new strategies may be proposed in the design of different crystal structures [44].

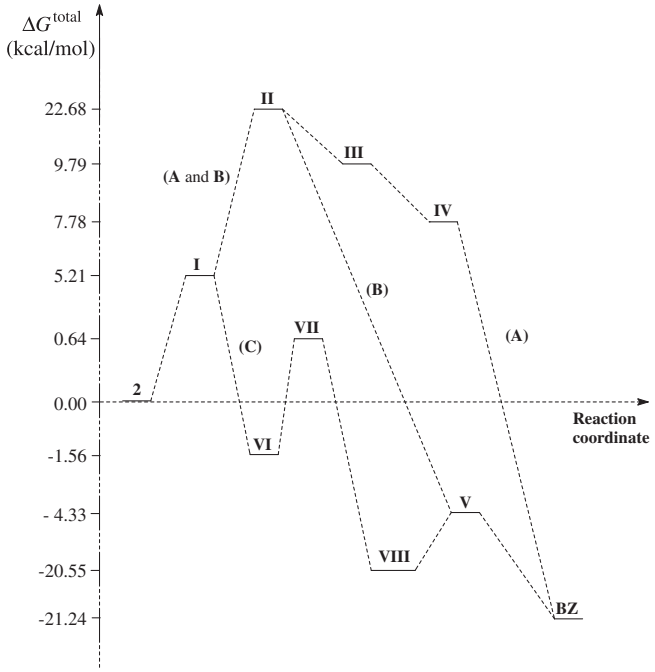

Fig. 6. Energy variation (in kcal/mol) of the sequences of reaction steps (sequences A–C) to the formation of **BZ** from **2**, as shown in Fig. 5, obtained from DFT/BLYP/6-31G* calculated values considering solvent effect (DMSO) using PCM model (Table 5).

The literature describes the decomposition of oxamic acids in the presence of Fe^{3+} or Gd^{3+} [45,46]. In both of these cases, the mechanisms and reaction steps are not known. However, the formation of oxalate and *ortho*-phenylenediamine has been proposed from the hydrolysis of **1** in the presence of Gd^{3+} or oxamides in the presence of Fe^{3+}. Recently, it was observed that a novel transition metal induced derivatization. The Cu^{2+} ion is not coordinated by the ligands diethyl *N*,*N*′-anthra-9,10-chinone-1,2-bis(oxamate) and diethyl *N*,*N*′-4,5-dinitro-*o*-phenylene-bis(oxamate) in the mode $\eta^4(\kappa^2N, \kappa^2O)$ as usually observed in $[bis(oxamato)]^{4-}$ ligands [47]. In contrast, in this work, the decomposition of **2** was verified in DMSO without the presence of transition metal ions.

Three reaction sequences may be proposed to the formation of **BZ** from **2**: sequence A (**2** → **I** → **II** → **III** → **IV** → **BZ**), sequence B (**2** → **I** → **II** → **V** → **BZ**), and sequence C (**2** → **I** → **VI** → **VII** → **VIII** → **V** → **BZ**), as seen in Fig. 5. In the first reaction step, all sequences provide **I** from the hydrolysis of an amide group of **2**. In fact, amides may be hydrolyzed in acid [48,49] or basic [50] media. In both media, the reaction is essentially irreversible. In neutral media hydrolyzes of amides have been also observed, but these reactions occur very slowly [51]. In the sequences A and B, the intermediate **I** can undergo nucleophilic attack by nitrogen of the amine group to the carbonylic carbon of the amide group, a cyclization that gives intermediate **II**.

In sequence A, the formation of the intermediate **III** occurs from the dehydration of **II**, as that exhibited to the formation of imines from carbonylic compounds [52–54]. Next, intermediate **III** undergoes decarboxylation, giving **IV**, and finally prototropic tautomerism of intermediate **IV** provides the product **BZ**. In fact, many carboxylic acids can be successfully decarboxylated, giving either a free acid or the corresponding acid salt form [55]. The decarboxylation of these compounds is favored when the structure has functional groups, mainly double or triple bond, placed at the α- or β-position. The mechanisms S_E1 or S_E2 have been suggested for the decarboxylation [56,57]. Moreover, some acids can be decarboxylated through a cyclic six-center mechanism [58,59]. In the case of aromatic acids, the decarboxylation can take place by the arenium ion mechanism, in which H^+ is the electrophile and CO_2 is the leaving group [60–63]. In the case of the S_E1 mechanism, the reaction is assisted by the presence of electron-withdrawing groups, which stabilize the carbanion formed [64,65]. The evidences for this S_E1-type mechanism are that the reaction is first order and electron-withdrawing groups, which would stabilize the carbanion, facilitate the reaction [66]. The decarboxylation of

Table 5
Electronic plus nuclear repulsion energy (E^{electr}), solvation energy (E^{solv}), total energy (G^{total}), and entropy (S) calculated for the structures involving in formation of **BZ** from **2** using the DFT/BLYP/6-31G* level of theory.

Structure	E^{electr} (Hartree)	E^{solv} (Hartree)	S (cal/mol K)	G^{total} (Hartree)
2	−946.55156779	−0.026517041	130.070	−946.417894
BZ	−379.719417943	−0.018116071	79.010	−379.635127
I	−644.667860025	−0.026060483	107.724	−644.552270
II	−644.641971314	−0.028594533	101.980	−644.524431
III	−568.251885370	−0.042667284	95.492	−568.158442
IV	−379.673336741	−0.021498955	79.127	−379.588892
V	−456.102570774	−0.021846929	88.091	−455.994710
VI	−342.805624072	−0.015012614	81.704	−342.705746
VII	−532.503663605	−0.022481914	100.187	−532.373364
VIII	−456.12615419	−0.020824614	93.909	−456.021177
H_2O	−76.3885439037	−0.011449664	46.590	−76.386526
$HO_2C—CO_2H$	−378.26118494	−0.017820002	74.340	−378.243842
HCO_2H	−189.720585411	−0.014364458	59.478	−189.671199
CO_2	−188.563059929	−0.003073239	51.342	−188.572757

carboxylate ions is favored in the presence of metallic ions [67], but the reaction has been also performed in its absence [68]. The decarboxylation of carboxylic acids has been also verified in wet DMSO [69–73].

In the third step of the sequence B, the formation of the intermediate **V** occurs from the decarboxylation of the intermediate **II**, followed by the dehydration of the intermediate and the obtainment of **BZ**. On the other hand, sequence C shows the hydrolysis of the intermediate **I** to formation of the intermediate **VI**. After, the condensation between intermediate **VI** and formic acid (which can be generated from the decomposition of the oxamic acid) provides intermediate **VII**. This latter intermediate undergoes dehydration to give the intermediate **VIII**, which undergoes intramolecular condensation to provide the intermediate **V**. The formation of **BZ** from the intermediate **V** would be similar to that proposed in sequence B.

DFT/BLYP/6-31G* geometry optimizations were performed for all structures shown in Fig. 5, considering calculations in the gaseous phase. Fig. 6 shows the energy variation to the sequences A, B, and C, which was obtained from the thermodynamic data shown in Table 5. The thermodynamic data shows that the formation of **BZ** from **2** is more favored through sequence C.

5. Conclusion

The experimental conditions for the synthesis of *ortho*-phenylenobis(oxamic acid) (**2**) and its derivative hydrogeno *ortho*-phenylenebis(oxamato) benzimidazolium (**3**) have been disclosed. Compound **2** was synthesized from a dilute solution of **1**, in order to prevent formation of polymeric impurities. In spite of the NMR data indicating the existence of two conformations for **2** in solution, the B3LYP/6-31G* calculations suggest that the lowest energy conformation is **2a** due to the hydrogen bonding between the hydrogen of the amide group of a substituent and the oxygen of the amide group of the other one. Despite crystal packing affects, especially the interaction between **H_3opba** and **BZ**, the weak N7—H71—O2 is also observed in the crystal structure of **3**. On the other hand, the B3LYP/6-31G* carbon chemical shift calculations indicate that the predominant conformer is **2b**.

The crystal structure of **3** was solved by X-ray diffraction. The structure is mainly stabilized by hydrogen bonds and π–π interactions. It seems that helical unidimensional supramolecular system plays a fundamental role in the crystal formation and stability. HF/3-21G* geometry optimizations for a *meso*-helical polymer chain containing 20 units of **3** indicated that van der Waals, electrostatic interactions, hydrogen bonding, and π–π interchain interactions must certainly play a key role in the aggregation of the polymeric units to provides the *meso*-helical crystal structure.

During the formation of **3** a proton is transferred from *ortho*-phenylenebis(oxamic acid) to benzymidazole group. This product is similar to the blend of adipic acid and benzymidazole which shows proton conductivity through a diffusion process within protonated and unprotonated benzymidazole groups. Compound **3** has a structure that makes it a potential candidate for water-free organic electrolyte systems.

Acknowledgments

The authors thank the Conselho Nacional de Desenvolvimento Científico e Tecnológico (CNPq), the Fundação Coordenação de Aperfeiçoamento de Pessoal de Nível Superior (CAPES), and the Fundação de Amparo à Pesquisa do Estado de Minas Gerais (FAPEMIG) for financial support. Authors would also like to thank Dr. Jason G. Taylor (Universidade Federal de Ouro Preto) for insightful discussion and for reviewing the manuscript for its English usage.

Appendix A. Supplementary data

Tables with the geometric parameters, figures with liner fit curves, and other results of all the optimized structures considered in this work are available from the authors upon request. Crystallographic data are deposited on Cambridge Crystallographic Data Center (CCDC 843697)

References

[1] B.V. Cheney, R.E. Christoffersentl, J. Med. Chem. 26 (1983) 726.
[2] B.V. Cheney, D.J. Duchamp, R.E. Christoffersentl, J. Med. Chem. 26 (1983) 719.
[3] J.B. Wright, C.M. Hall, H.G. Johnson, J. Med. Chem. 21 (1978) 930.
[4] O. Kahn, Angew. Chem. Int. Ed. Engl. 24 (1985) 834.
[5] O. Guillou, O. Kahn, R.L. Oushoorn, K. Boubekeurand, P. Batail, Inorg. Chim. Acta 198–200 (1992) 119.
[6] H.O. Stumpf, L. Ouahab, Y. Pei, P. Bergerat, O. Kahn, Science 261 (1993) 447.
[7] Y. Pei, M. Verdaguer, O. Kahn, J.P. Renard, J. Am. Chem. Soc. 108 (1986) 7428.
[8] O. Kahn, Y. Pei, J. Sletten, J. Am. Chem. Soc. 108 (1986) 3143.
[9] C.L.M. Pereira, E.F. Pedroso, M.A. Novak, A.L. Brandl, M. Knobel, H.O. Stumpf, Polyhedron 22 (2003) 2387.
[10] M.G.F. Vaz, M. Knobel, N.L. Speziali, A.M. Moreira, A.F.C. Alcântara, H.O. Stumpf, J. Brazil Chem. Soc. 13 (2002) 183.
[11] M.G.F. Vaz, J.D. Ardisson, N.L. Speziali, G.P. Souza, H.O. Stumpf, M. Knobel, W.A.A. Macedo, Polyhedron 20 (2001) 1431.
[12] O. Kahn, H. Stumpf, Y. Pei, J. Sletten, Mol. Cryst. Liq. Cryst. 233 (1993) 231.
[13] R. Ruiz, J. Faus, F. Lloret, M. Julve, Y. Journaurx, Coord. Chem. Rev. 193–195 (1999) 1069.
[14] H.O. Stumpf, Y. Pei, O. Kahn, J. Sletten, J.-P. Renard, J. Am. Chem. Soc. 115 (1993) 6738.
[15] E. Pardo, F. Lloret, R. Carrasco, M.C. Muñoz, T. Temporal-Sánchez, R. Ruiz-García, Inorg. Chim. Acta 357 (2004) 2713.
[16] G.P. Souza, C. Konzen, J.D. Ardisson, H.A. De Abreu, H.A. Duarte, A.F.C. Alcantara, W.C. Nunes, W.A.A. Macedo, M. Knobel, H.O. Stumpf, J. Brazil Chem. Soc. 17 (2006) 1534.
[17] M.C. Munõz, G. Blay, I. Fernández, Cryst. Eng. Comm. 12 (2010) 2473.
[18] L. Frkanec, M. Zinic, Chem. Commun. 46 (2010) 522.
[19] J. Makarevic, M. Jokic, Z. Raza, Z. Stefanic, B. Kojic-Prodic, M. Zinic, Chem. Eur. J. 9 (2003) 5567.
[20] J.S. Binkley, J.A. Pople, W.J. Hehre, J. Am. Chem. Soc. 102 (1980) 939.
[21] R.G. Parr, W. Yang, Density Functional Theory of Atoms and Molecules, New York, Oxford, 1989.
[22] A.M. Barreto, A.F.C. Alcântara, H. Beraldo, Tetrahedron 61 (2005) 7045.
[23] A.F.C. Alcântara, D. Piló-Veloso, W.B. De Almeida, C.R.A. Maltha, L.C.A. Barbosa, J. Mol. Struct. 791 (2006) 180.
[24] S. Pausak, A. Pines, J.S. Waugh, J. Chem. Phys. 59 (1973) 591.
[25] Nonis, Collect, Data collecting software, Nonius BV, 1999.
[26] Z. Otowinowski, W. Minor, Methods in Enzymologyin: C.W. Cart Jr., R.M. Sweet (Eds.), Macromolecular Crystallography, Part A, vol. 276, Academic Press, New York, pp. 307–326.
[27] G.M. Sheldrick, SHELX97, Program for the Refinement of Crystal Structures, University of Göttingen, Germany, 1997.
[28] M.J. Frisch, G.W. Trucks, H.B. Schlegel, G.E. Scuseria, M.A. Robb, J.R. Cheeseman, J.A. Montgomery, T. Vreven, K.N. Kudin, J.C. Burant, J.M. Millam, S.S. Iyengar, J. Tomasi, V. Barone, B. Mennucci, M. Cossi, G. Scalmani, N. Rega, G.A. Petersson, H. Nakatsuji, M. Hada, M. Ehara, K. Toyota, R. Fukuda, J. Hasegawa, M. Ishida, T. Nakajima, Y. Honda, O. Kitao, H. Nakai, M. Klene, X. Li, J.E. Knox, H.P. Hratchian, J.B. Cross, C. Adamo, J. Jaramillo, R. Gomperts, R.E. Stratmann, O. Yazyev, A.J. Austin, R. Cammi, C. Pomelli, J.W. Ochterski, P.Y. Ayala, K. Morokuma, G.A. Voth, P. Salvador, J.J. Dannenberg, V.G. Zakrzewski, S. Dapprich, A.D. Daniels, M.C. Strain, O. Farkas, D.K. Malick, A.D. Rabuck, K. Raghavachari, J.B. Foresman, J.V. Ortiz, Q. Cui, A.G. Baboul, S. Clifford, J. Cioslowski, B.B. Stefanov, G. Liu, A. Liashenko, P. Piskorz, I. Komaromi, R.L. Martin, D.J. Fox, T. Keith, M.A. Al-Laham, C.Y. Peng, A. Nanayakkara, M. Challacombe, P.M.W. Gill, B. Johnson, W. Chen, M.W. Wong, C. Gonzalez, J.A. Pople, GAUSSIAN 2003, Revision B.04, Gaussian, Inc., Pittsburgh PA, 2003.
[29] M.J.S. Dewar, E.G. Zoebish, E.F. Healy, J.J.P. Stewart, J. Am. Chem. Soc. 107 (1985) 3902.
[30] R. Ditchfield, W.J. Hehre, J.A. Pople, J. Chem. Phys. 54 (1971) 724.
[31] W.J. Hehre, R. Ditchfield, J.A. Pople, J. Chem. Phys. 56 (1972) 2257.
[32] P.C. Hariharan, J.A. Pople, Mol. Phys. 27 (1974) 209.
[33] M.S. Gordon, Chem. Phys. Lett. 76 (1980) 163.
[34] C. Hariharan, J.A. Pople, Theor. Chim. Acta 28 (1973) 213.
[35] M. Cossi, V. Barone, R. Camimi, J. Tomasi, Chem. Phys. Lett. 255 (1996) 327.
[36] V. Barone, M. Cossi, J. Tomasi, J. Chem. Phys. 107 (1997) 3210.
[37] S. Ueda, T. Fukunagaa, H. Ishidab, Acta Cryst. E61 (2005) 1845.
[38] B. Karadedeli, A. Bozkurt, A. Baykal, Physica B 364 (2005) 279.
[39] Z. Chen, C. Zhang, L. Feng, Spectrochim. Acta Part A 62 (2005) 592.
[40] B. Moulton, M.J. Zaworotko, Chem. Rev. 101 (2001) 1629.
[41] L.M. Greig, D. Philp, Chem. Soc. Rev. 30 (2001) 287.
[42] G. Blay, I. Fernández, J.R. Pedro, R. Ruiz-Garcia, M.C. Munoz, J. Cano, R. Carrasco, Eur. J. Org. Chem. 2003 (2003) 1627.
[43] G. Yang, X.-L. Yu, Cryst. Res. Technol. 35 (2000) 993.

[44] G.R. Desiraju, Angew. Chem. Int. Engl. 34 (1995) 2311.
[45] M.C. Muñoz, R. Ruiz-Garcıa, M. Traianidis, A. Aukauloo, J. Cano, Y. Yournaux, I. Fernandez, J.R. Pedro, Angew. Chem. Int. Engl. 37 (1998) 1833.
[46] O. Guillou, P. Bergerat, O. Kahn, E. Bakalbassis, K. Boubekeur, P. Batail, M. Guillot, Inorg. Chem. 31 (1992) 110.
[47] T. Rüffer, B. Bräuer, F.E. Meva, B. Walfort, Dalton Trans. 37 (2008) 5089.
[48] R.A. McClelland, J. Am. Chem. Soc. 97 (1975) 5281.
[49] A.J. Bennet, H. Slebocka-Tilk, R.S. Brown, J.P. Guthrie, A. Jodhan, J. Am. Chem. Soc. 112 (1990) 8497.
[50] R.H. De Wolfe, R.C. Newcomb, J. Org. Chem. 36 (1971) 3870.
[51] D. Kahne, W.C. Still, J. Am. Chem. Soc. 110 (1988) 7529.
[52] A.F.C. Alcântara, D. Piló-Veloso, D.L. Nelson, J. Brazil Chem. Soc. 7 (1996) 225.
[53] J.R. Pliego Jr., A.F.C. Alcântara, D. Piló-Veloso, W.B. De Almeida, J. Brazil Chem. Soc. 10 (1999) 381.
[54] A.F.C. Alcântara, H.F. Santos, W.B. De Almeida, M.G.F. Vaz, L.M.M. Pinheiro, H.O. Stumpf, Struct. Chem. 10 (1999) 367.
[55] J. March, J. Chem. Educ. 40 (1963) 212.
[56] S.P. Singh, J. Kagan, J. Org. Chem. 35 (1970) 2203.
[57] V.J. Shiner, B. Martin, J. Am. Chem. Soc. 84 (1962) 4824.
[58] D.B. Bigley, M.F. Clarke, J. Chem. Soc. Perkin Trans. 2 (1982) 1.
[59] G.G. Smith, F.W. Kelly, Prog. Phys. Org. Chem. 8 (1971) 75.
[60] D.B. Bigley, J. Chem. Soc. (1964) 3897.
[61] G.L. Buchanan, N.B. Kean, R. Taylor, Tetrahedron 31 (1975) 1583.
[62] H.H. Huang, F.A. Long, J. Am. Chem. Soc. 91 (1969) 2872.
[63] A.V. Willi, M.H. Cho, C.M. Won, Helv. Chim. Acta 53 (1970) 663.
[64] S. Oae, W. Tagaki, K. Uneyama, I. Minamida, Tetrahedron 24 (1968) 5283.
[65] E. Buncel, T.K. Venkatachalam, B.C. Menon, J. Org. Chem. 49 (1984) 413.
[66] P. Segura, J.F. Bunnett, L. Villanova, J. Org. Chem. 50 (1985) 1041.
[67] D.H. Hunter, V. Patel, R.A. Perry, Can. J. Chem. 58 (1980) 2271.
[68] S.T. Graul, R.R. Squires, J. Am. Chem. Soc. 110 (1988) 607.
[69] A.P. Krapcho, Synthesis 805–822 (1982) 893.
[70] R. Aneja, W.M. Hollis, A.P. Davies, G. Eaton, Tetrahedron Lett. 24 (1983) 4641.
[71] R.T. Brown, M.F. Jones, J. Chem. Res. (S) (1984) 332.
[72] E.V. Dehmlow, E. Kunesch, Synthesis (1984) 320.
[73] D.F. Taber, J.C. Amedio, F. Gulino, J. Org. Chem. 54 (1989) 3474.